Journal of Nuclear Medicine, published on October 7, 2022 as doi:10.2967/jnumed.122.264749

Preclinical evaluation of ^{68}Ga- and ^{177}Lu-labeled integrin $\alpha_v\beta_6$-targeting radiotheranostic peptides

Tanushree Ganguly[1], Nadine Bauer[2], Ryan A. Davis[1], Cameron C. Foster[3], Rebecca E. Harris[2], Sven H. Hausner[2], Emilie Roncali[1,3], Sarah Y. Tang[2], Julie L. Sutcliffe[1, 2, 4]

1. *Department of Biomedical Engineering; University of California Davis, Davis, CA, USA*
2. *Department of Internal Medicine, Division of Hematology/Oncology; University of California Davis, Sacramento, CA, USA*
3. *Department of Radiology, Division of Nuclear Medicine; University of California Davis, Sacramento, CA, USA*
4. *Center for Molecular and Genomic Imaging; University of California Davis, Davis, CA, USA*

CORRESPONDING AUTHOR: Prof. Julie L. Sutcliffe
University of California Davis Medical Center
2921 Stockton Boulevard,
Institute for Regenerative Cures, Room 1763
Sacramento, CA, 95817
tel: (916) 734-5536
fax: (916) 734-7572
jlsutcliffe@ucdavis.edu

FIRST AUTHOR: Dr. Tanushree Ganguly
Assistant Project Scientist
University of California Davis Medical Center
2921 Stockton Boulevard,
Institute for Regenerative Cures, Room 1761
Sacramento, CA, 95817
tel: (916) 734-5482
tganguly@ucdavis.edu

RUNNING TITLE: Theranostic peptides for integrin $\alpha_v\beta_6$

WORD COUNT: 5039

This work was supported by Stand Up To Cancer and Lustgarten Foundation Pancreatic Cancer Collective (PCC) New Therapies Challenges (SU2C-AACR-PCC-06-18).

S. H. Hausner is a co-inventor of intellectual property related to **1** and **2**. J. L. Sutcliffe is founder and CEO of and holds owner-ship interest (including patents) in Luminance Biosciences, Inc., and is a co-inventor of intellectual property related to **1** and **2**.

ABSTRACT

Rationale: The integrin $\alpha_v\beta_6$, an epithelial-specific cell surface receptor, is overexpressed on numerous malignancies, including the highly lethal pancreatic ductal adenocarcinomas (PDAC). Here, we developed and tested a novel $\alpha_v\beta_6$-targeting peptide, DOTA-5G (**1**) radiolabeled with gallium-68 for positron emission tomography/computed tomography (PET/CT) imaging, and lutetium-177 for treatment. With the goal to develop a radiotheranostic, further modifications were made for increased circulation time, renal recycling, and tumor uptake, yielding DOTA-ABM-5G (**2**).

Methods: Peptides **1** and **2** were synthesized on solid phase and their affinity for $\alpha_v\beta_6$ assessed by ELISA. The peptides were radiolabeled with gallium-68 and lutetium-177. *In vitro* cell binding, internalization, and efflux of ^{68}Ga-**1** and ^{177}Lu-**2** were evaluated in $\alpha_v\beta_6$ (+) BxPC-3 human pancreatic cancer cells. PET/CT imaging of ^{68}Ga-**1** and ^{68}Ga-**2** was performed in female nu/nu mice bearing subcutaneous BxPC-3 tumors. Biodistribution was performed for ^{68}Ga-**1** (1 and 2 h p.i.), ^{68}Ga-**2** (2 and 4 h p.i.), and ^{177}Lu-**1** and ^{177}Lu-**2** (1, 24, 48, and 72 h p.i.). The ^{177}Lu-**2** biodistribution data were extrapolated for human dosimetry data estimates using OLINDA/EXM 1.1. Therapeutic efficacy of ^{177}Lu-**2** was evaluated in mice bearing BxPC-3 tumors.

Results: Peptides **1** and **2** demonstrated high affinity (< 55 nM) for $\alpha_v\beta_6$ by ELISA. ^{68}Ga-**1**, ^{68}Ga-**2**, ^{177}Lu-**1** and ^{177}Lu-**2** were synthesized in high radiochemical purity (RCP). Rapid *in vitro* binding and internalization of ^{68}Ga-**1** and ^{177}Lu-**2** were observed in BxPC-3 cells. PET/CT imaging and biodistribution studies demonstrated uptake in BxPC-3 tumors. Introduction of the ABM in ^{177}Lu-**2** resulted in a 5-fold increase in tumor uptake and retention over time. Based on the extended dosimetry data the dose-limiting organ for ^{177}Lu-**2** are the kidneys. Treatment with ^{177}Lu-**2** prolonged median survival by 1.5-2 folds vs. controls.

Conclusions: ^{68}Ga-**1** and ^{177}Lu-**2** demonstrated high affinity for the integrin $\alpha_v\beta_6$ both *in vitro* and *in vivo*, were rapidly internalized into BxPC-3 cells, and were stable in mouse and human serum. Both radiotracers showed

favorable pharmacokinetics in pre-clinical studies with predominantly renal excretion and good tumor-to-normal tissue ratios. Favorable human dosimetry data suggest the potential of ^{177}Lu-**2** as a treatment for PDAC.

KEYWORDS: integrin $\alpha_v\beta_6$; Ga-68; Lu-177; theranostics; albumin-binding moiety

INTRODUCTION

Despite exhaustive testing and some encouraging advances in first- and second-line treatments, pancreatic ductal adenocarcinoma (PDAC) remains the fourth leading cause of cancer-related deaths with a 5-year survival below 10% (*1,2*). This dire reality is also in part due to diagnosis at an advanced stage of the disease and the poor reliability of current standard imaging approaches. Therefore, there clearly remains an urgent unmet clinical need for more effective molecularly targeted diagnostics and therapeutics.

The heterodimeric transmembrane receptor integrin $\alpha_v\beta_6$ has been identified as a potential molecular target; it is an epithelial-specific cell surface receptor that is undetectable in healthy adult epithelium but is significantly up-regulated in a wide range of epithelial-derived cancers, including PDAC (*3-10*). In fact, $\alpha_v\beta_6$ was initially identified in PDAC with nearly uniform high expression among patient samples screened; moreover, metastatic lesions demonstrate further highly upregulated expression of $\alpha_v\beta_6$ when compared to the primary tumor, and $\alpha_v\beta_6$ is undetectable in normal pancreas (*11*). These traits further underscore the potential of $\alpha_v\beta_6$ as an attractive target for both the early detection and targeted delivery of a therapeutic payload in PDAC.

Radiotheranostics combines molecular imaging with targeted radionuclide therapy, often using the same targeting ligand, and has shown efficacy in several cancers (*12,13*). Over the last few years we have seen an exponential growth in the development and acceptance of radiotheranostics for applications in oncology. For example ^{68}Ga-DOTATATE for imaging of neuroendocrine tumors (NETs) and ^{177}Lu-DOTATATE for peptide receptor radionuclide therapy (PRRT) were the first radiotheranostic peptides to be approved by the FDA in 2018 (*14*). More recently ^{18}F-DCFPyL and ^{68}Ga-PSMA-11 gained approval for imaging, and ^{177}Lu-PSMA-617 for treatment of prostate-specific membrane antigen (PSMA)-positive metastatic castration resistant prostate cancer (CRPC) (*15*).

Several groups including our own have developed molecular imaging agents to target the integrin $\alpha_v\beta_6$, and a number of promising agents have advanced to clinical trials for imaging cancer and fibrosis (*16-20*). Building on over a decade of work by the Sutcliffe laboratory to develop $\alpha_v\beta_6$ targeted molecular imaging agents (*17,21,22*) we now propose to address the clear unmet need for new therapies for PDAC using a radiotheranostic strategy. We present a novel molecularly targeted radiotheranostic approach via the integrin $\alpha_v\beta_6$ for PRRT.

DOTA-5G (**1**) was designed to selectively target the integrin $\alpha_v\beta_6$; in addition, with the goal to increase blood residence time, tumor uptake, and renal recycling, an albumin-binding moiety (ABM) was incorporated in the peptide to yield DOTA-ABM-5G (**2**). The peptides were synthesized on solid phase, labeled with gallium-68 ($t_{1/2}$ = 68 min, E_{β^+} (max) = 900 keV (23%)) for imaging and lutetium-177 ($t_{1/2}$ = 6.7 days, E_{β^-} (max) = 490 keV, E_γ = 208 keV (11%)) for therapy, and evaluated *in vitro* (for cell binding, internalization, and efflux) in $\alpha_v\beta_6$-expressing BxPC-3 human pancreatic cancer cells. Albumin binding and stability in mouse and human serum were determined. *In vivo* PET/CT imaging and biodistribution studies were performed in mice bearing BxPC-3 tumors xenografts, and $\alpha_v\beta_6$-specific targeting was confirmed by blocking studies. Human dosimetry was estimated from the extended biodistribution data, and therapeutic efficacy was evaluated in mice bearing BxPC-3 tumors.

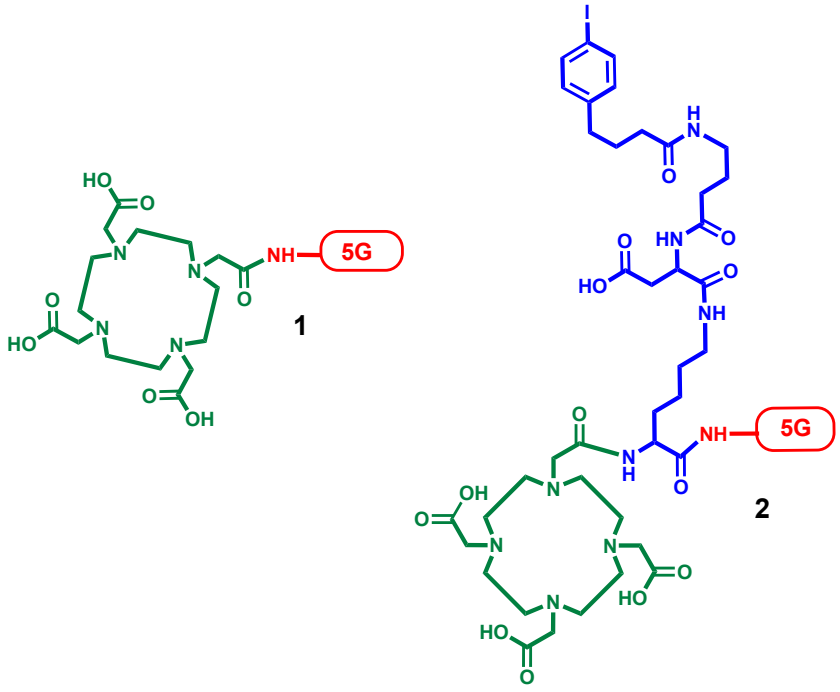

FIGURE 1. Chemical structures of **1** and **2**. The peptide is indicated in red, the DOTA chelator in green, and the ABM in blue.

MATERIALS AND METHODS

Chemistry and Radiochemistry

Peptide synthesis on solid phase (*23*) and radiolabeling and formulation of ^{68}Ga- and ^{177}Lu-labeled peptides are described in the Supplemental Section 2.

In Vitro Experiments

ELISAs (*23,24*); cell binding, and internalization; albumin binding (*23*); and serum stability (*25*) followed previously published procedures as described in the Supplemental Section 3.

In Vivo Imaging, Biodistribution and Targeted Radionuclide Therapy

All animal studies were and carried out according to procedures approved by the UC Davis Institutional Animal Care and Use Committee. BxPC-3 cells (5×10^6) were implanted subcutaneously into the left shoulder of 6–8 week old female nu/nu nude mice (Charles River Laboratories, Wilmington, MA, USA) and allowed to grow for 3 weeks (imaging and biodistribution) and approximately 2 weeks (therapy).

For imaging, the radiotracer (^{68}Ga-**1** or ^{68}Ga-**2**, 7.4–9.25 MBq) in PBS solution (150 µL, pH 7.2) was injected intravenously (i.v.) into the tail vein of mice (n=3/time point/radiotracer) anesthetized with 3% isoflurane in medical grade oxygen. Following a conscious uptake periods of 1 and 2 h, the animals were anesthetized and imaged two at a time, side by side in a feet-first prone position as previously described (*26*).

For biodistribution, the radiotracer (3-3.7 MBq in 100 µL PBS) was injected into the tail vein, followed by conscious uptake periods of 1 and 2 h (^{68}Ga-**1**), 2 and 4 h (^{68}Ga-**2**), or 1, 24, 48, and 72 h (^{177}Lu-**1** and ^{177}Lu -**2**). For blocking studies, the respective peptide (30 mg/kg, 10 mg/mL (**1**) and 48 mg/kg, 16 mg/mL (**2**) solution in PBS) was injected 10 min before the radiotracer. At each time point, the mice (n=3/time point/radiotracer) were anesthetized and sacrificed, tissues were collected, rinsed with PBS, and the radioactivity measured with a gamma counter. Radioactivity concentrations were calibrated, decay-corrected, and expressed as percentage of injected dose per gram of tissue (%ID/g).

An extended biodistribution study was performed for ^{177}Lu -**2**. 3.7 – 5.55 MBq in 100 µl PBS were injected into the tail vein of male (n=4 per time point) and female (n=4 per time point) mice, followed by conscious uptake periods of 24 h, 48 h, 72 h, 1 week and 2 weeks. The dosimetry values for ^{177}Lu -**2** were computed using OLINDA/EXM1.1 using a female or male model with organ mass scaling and effective doses reported as mSv/MBq.

For the therapeutic efficacy study, mice were randomly chosen and divided into four treatment groups – Control Saline (Group 1, n = 5), Control Peptide **2** (Group 2, n = 6), 74 MBq ^{177}Lu-**2** (Group 3, n = 10) and 2 × 37 MBq ^{177}Lu-**2** (Group 4, n = 7). Tumor volumes at the start of the treatment ranged from 14 to 218 mm^3. Group 2 received 20 µg of peptide **2**, Group 3 received a single dose of 74 MBq (20 µg of peptide **2**) on day 14 post tumor implant (treatment day 0), and Group 4 received one dose of 37 MBq (10 µg of peptide **2**) on each, day 14 and 21 post tumor implant (treatment days 0 and 7). Body weights and tumor volumes were measured the day before treatment, and twice a week post treatment throughout the study.

Statistical Analysis

All statistical data are reported as mean ± standard deviation (SD). Paired, two-tailed Student's t-tests were used to evaluate statistical significance, where $p < 0.05$ was considered statistically significant.

RESULTS

Synthesis of 1 and 2 and Respective ^{nat}Ga and ^{nat}Lu Analogs

Peptides **1** and **2** were synthesized by solid phase peptide synthesis and obtained in high purity (>98%) after HPLC purification, and ^{nat}Ga-**1**, ^{nat}Ga-**2**, ^{nat}Lu-**1** and ^{nat}Lu-**2** were obtained in ≥98% purity. The analytical data are provided in Supplemental Section 2. ^{nat}Ga-**1**, ^{nat}Ga-**2**, ^{nat}Lu-**1** and ^{nat}Lu-**2** were used in ELISA for IC_{50} determination, and as reference standards for HPLC co-injection to confirm the identity of the ^{68}Ga- and ^{177}Lu-labeled peptides.

Radiochemical Synthesis

^{68}Ga-**1** and ^{68}Ga-**2** were obtained in ≥98% radiochemical purity (RCP) after semipreparative HPLC purification. ^{177}Lu-**1** and ^{177}Lu-**2** were obtained in ≥97% RCP.

IC_{50} Determinations

The IC_{50} of ^{nat}Ga-**1**, ^{nat}Ga-**2**, ^{nat}Lu-**1** and ^{nat}Lu-**2** for integrin $\alpha_v\beta_6$ determined by ELISA were 33.2 ± 1.5 nM, 37.2 ± 3.5 nM, 50.0 ± 4.4 nM, and 29.0 ± 0.6 nM, respectively. The binding affinities for integrin $\alpha_v\beta_3$ were >100 μM for all peptides.

Cell binding, Internalization and Efflux

For ^{68}Ga-**1**, 16.1 ± 0.3% of total radioactivity bound to the BxPC-3 cells, of which 71.5 ± 0.6% internalized into the cells. For ^{177}Lu-**2**, 31.5 ± 0.6% bound, of which 72.3 ± 1.0% internalized, and minimal efflux was observed for ^{177}Lu-**2** at 1 h (~20% of internalized radioactivity) (Figure 2).

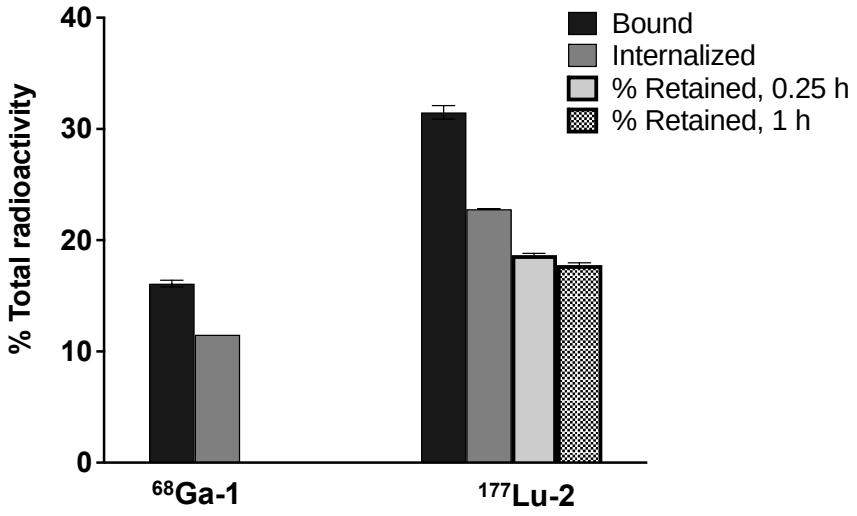

FIGURE 2. Cell-binding and internalization of ^{68}Ga-**1** and ^{177}Lu-**2** at 1 h to BxPC-3 cells at 37°C, and percentage radioactivity of ^{177}Lu-**2** retained in BxPC-3 cells post-internalization. Internalization is expressed as fraction of total radioactivity (n = 3/radiotracer; 1 h incubation).

Albumin binding

Albumin binding of ^{177}Lu-**2** was 54.4 ± 2.8% and 58.1 ± 0.4% for mouse and human serum, respectively, compared to 18.1 ± 0.2% and 16.2 ± 0.4%, respectively, for ^{177}Lu-**1**.

Serum Stability

^{68}Ga-**1** and ^{68}Ga-**2** were 100% intact at 2 h in both mouse and human serum. At 24 h, ^{177}Lu-**1** and ^{177}Lu-**2** were 72% and 78% intact, respectively, in mouse serum, and ≥97% intact (both) in human serum.

***In vivo* imaging and biodistribution**

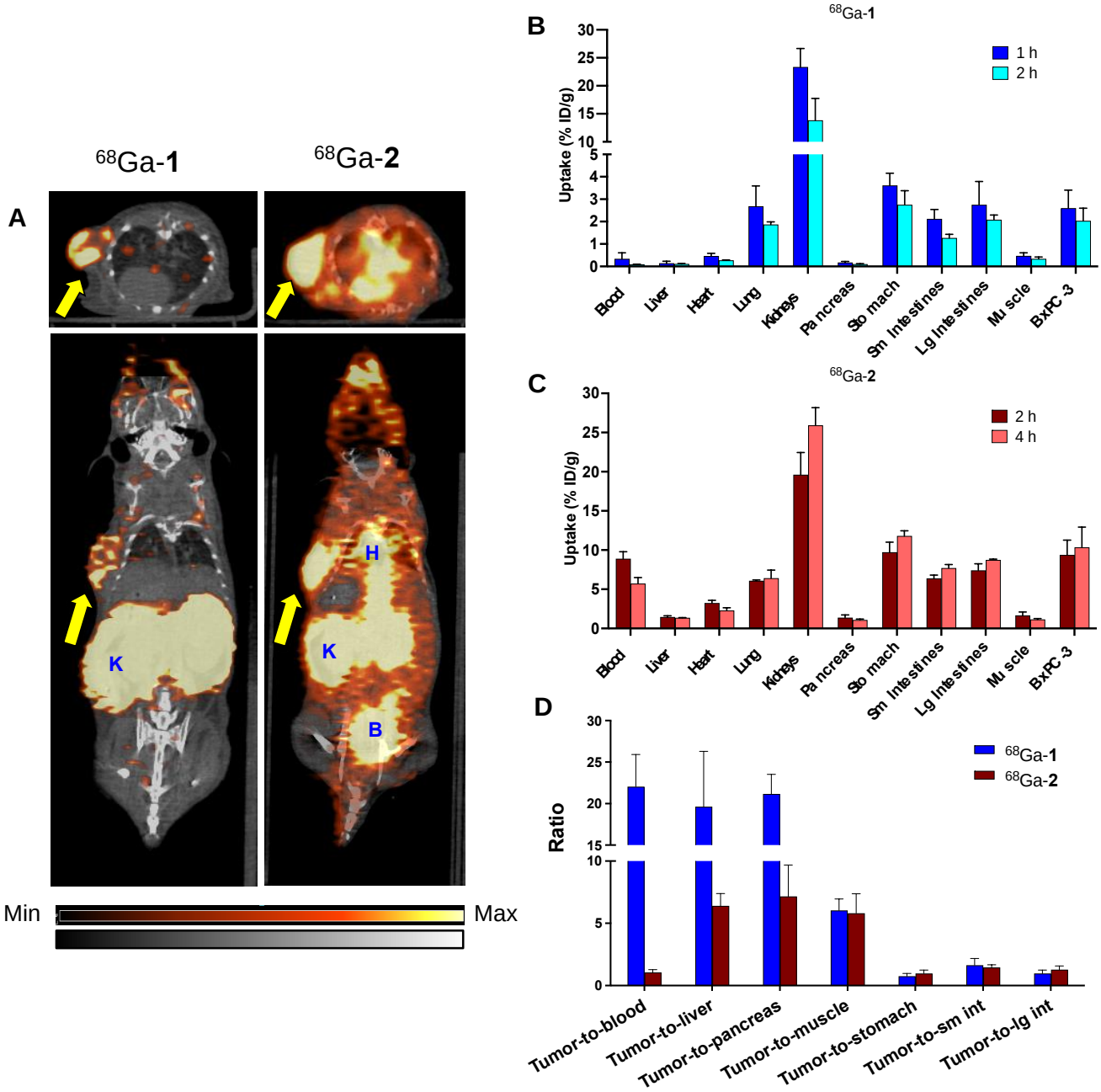

FIGURE 3. (A) Representative transaxial (top) and coronal (bottom) PET/CT cross sections of mice bearing BxPC-3 tumors (arrow) obtained at 2 h after injection (K-Kidney, B-Bladder, H-Heart; red = PET, gray = CT). Both images are presented on the same scale. Biodistribution showing uptake (%ID/g) of ^{68}Ga-**1** and ^{68}Ga-**2** (B

and C) in selected organs and $\alpha_v\beta_6$ (+) BxPC-3 tumors (n = 3/group/time point), and tumor-to-tissue ratios 2 h post injection (D).

*Imaging and Biodistribution of ^{68}Ga-**1** and ^{68}Ga-**2**.* Imaging and biodistribution were performed in the subcutaneous BxPC-3 tumor model at 1 and 2 h post injection (p.i.) for ^{68}Ga-**1**, and at 2 and 4 h p.i. for ^{68}Ga-**2** (Figure 3, Supplemental Table 1). Uptake and retention in the tumor was evident at all time points for both, ^{68}Ga-**1** and ^{68}Ga-**2**. However, while ^{68}Ga-**1** cleared from key organs such as kidneys by 2 h, uptake of ^{68}Ga-**2** continued to trend upwards. Tumor uptake was 2.6 ± 0.8% at 1 h and 2.0 ± 0.6% at 2 h p.i. for ^{68}Ga-**1**, and 9.4 ± 1.9% at 2 h and 10.4 ± 2.6% at 4 h p.i. for ^{68}Ga-**2**.

Renal uptake of ^{68}Ga-**1** was 23 ± 3 %ID/g at 1 h, dropping to 14 ± 4 %ID/g at 2 h ($p = 0.032$). For ^{68}Ga-**2**, renal uptake was 20 ± 3 %ID/g at 2 h, increasing to 26 ± 2 %ID/g at 4 h ($p = 0.039$). As depicted in Figure 3 D, tumor-to-organ ratios at 2 h p.i. for ^{68}Ga-**1** and ^{68}Ga-**2**, respectively, were: 0.75 ± 0.23 and 0.88 ± 0.25 (stomach), 1.6 ± 0.5 and 1.3 ± 0.3 (small intestine), 0.98 ± 0.26 and 1.2 ± 0.3 (large intestine), 20 ± 7 and 6 ± 0.9 (liver), 21 ± 2 and 7.2 ± 2.5 (pancreas), and 22 ± 3.9 and 1.1 ± 0.2 (blood). Collectively these data suggest that ^{68}Ga-1 has the most favorable biodistribution properties for a PDAC imaging agent, clearing rapidly from key organs whilst being retained by the tumor.

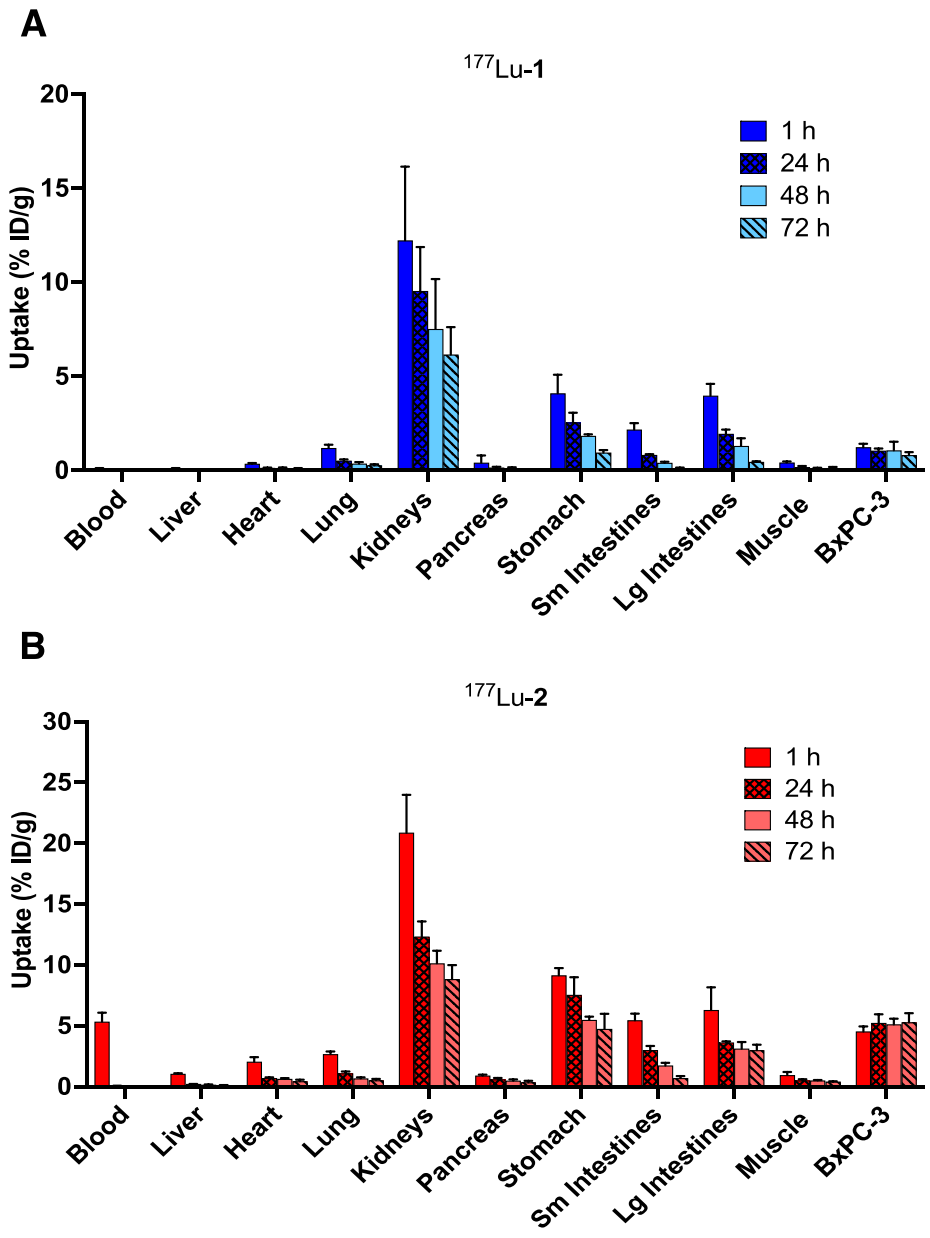

FIGURE 4. Biodistribution showing uptake (%ID/g) of ^{177}Lu-**1** and ^{177}Lu-**2** (A and B) in selected organs and $\alpha_v\beta_6$ (+) BxPC-3 tumors (n = 3/group/time point).

*Biodistribution of ^{177}Lu-**1** and ^{177}Lu-**2**.* Uptake and retention of ^{177}Lu-**2** in the BxPC-3 tumor was at least 4-fold greater than for ^{177}Lu-**1**, with ^{177}Lu-**2** remaining at 5 ± 0.8 %ID/g at 72 h (Figures 4, 5 Supplemental Tables 2 and 3). Both, ^{177}Lu-**1** and ^{177}Lu-**2** demonstrated wash out from key organs over time, resulting in tumor-to-kidney ratios for ^{177}Lu-**1** of 0.08 ± 0.05 (1 h) and 0.14 ± 0.05 (72 h), and for ^{177}Lu-**2** of 0.22 ± 0.05 (1

h) and 0.60 ± 0.02 (72 h) (Figure 5B). For the same time points, tumor-to-stomach ratios for ^{177}Lu-**1** were, respectively, 0.31 ± 0.06 and 0.87 ± 0.28, and for ^{177}Lu-**2** were 0.50 ± 0.08 and 1.16 ± 0.30 (Figure 5C). Likewise, tumor-to-pancreas ratios for ^{177}Lu-**1** were 5 ± 3 and 9 ± 1.4, and for ^{177}Lu-**2** were 5 ± 0.06 and 16 ± 5 (Figure 5D); and tumor-to-large intestine ratios for ^{177}Lu-**1** were 0.31 ± 0.02 and 1.74 ± 0.39, and for ^{177}Lu-**2** were 0.77 ± 0.25 and 1.77 ± 0.26. Collectively, these data suggest that ^{177}Lu-**2** has the most favorable pharmacokinetics to advance to therapeutic efficacy studies.

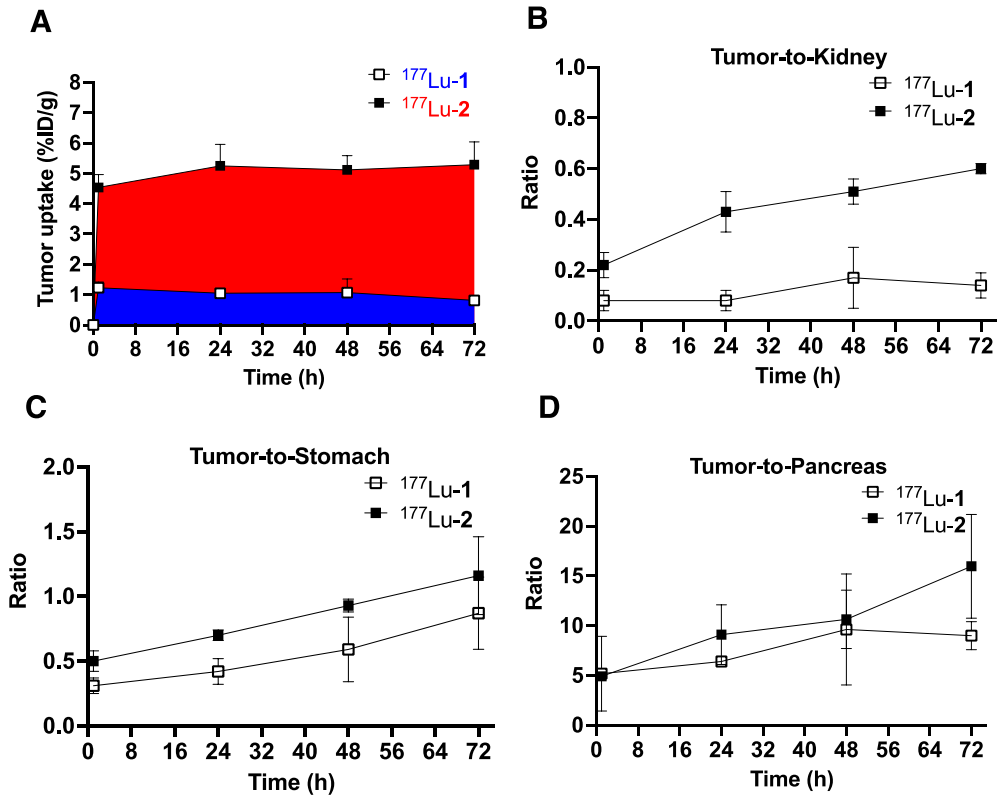

FIGURE 5. Uptake of ^{177}Lu-**1** and ^{177}Lu-**2** in BxPC-3 tumor (A), and tumor-to-organ ratios for kidney (B), stomach (C), and pancreas (D) derived from biodistribution data.

Blocking studies. Pre-administration of the respective blocking peptide (**1** or **2**) 10 min prior to administration of ^{68}Ga-**1**, ^{177}Lu-**1**, or ^{177}Lu-**2** resulted in reduced tumor uptake. Tumor uptake dropped from 2.6 ± 0.8 %ID/g (unblocked) to 0.27 ± 0.02 %ID/g for ^{68}Ga-**1** (1 h, Δ = -86%); for ^{177}Lu-**1** tumor uptake dropped from 1.2 ± 0.2 %ID/g to 0.3 ± 0.02 %ID/g (1 h, Δ = -75%); and for ^{177}Lu-**2** tumor uptake dropped from 7.2 ± 3.0

%ID/g to 4.1 %ID/g (4 h, Δ = -42%; Supplemental Figures 1-3).

Therapeutic efficacy

Significant delay in tumor growth was observed in treatment Groups 3 (74 MBq ^{177}Lu-**2**) and 4 (2 × 37 MBq ^{177}Lu-**2**) vs. the control Groups 1 and 2 (Figure 6A). All mice in the control Groups 1 and 2 had met the end point criteria (tumor ≥2 cm in any direction and/or ulceration) by day 63 and 68 from start of treatment, respectively. In contrast, the mice in Groups 3 and 4 had 30% and 43% survival rate, respectively, at the end of study (120 days; Figure 6B). The median survival was 56 days for mice in control Groups 1 and 2, versus 82 days for treatment Group 3, and 113 days for treatment Group 4. No evidence of treatment-related adverse effects (weight loss or signs of distress) was observed during the course of the study (Supplemental Figure 4).

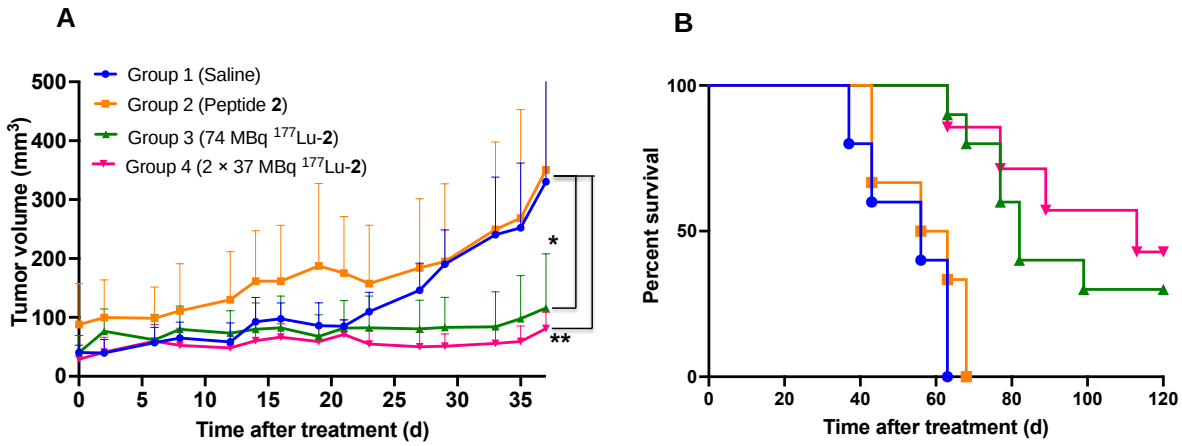

FIGURE 6. Therapeutic efficacy of ^{177}Lu-**2** in mice bearing $\alpha_v\beta_6$ (+) BxPC-3 tumors, as determined by (A) tumor growth (average tumor volume, up to 37 days post treatment; * p = 0.0077, ** p = 0.0064), and (B) survival data.

Dosimetry

The highest estimated dose, as expected from the imaging and biodistribution data, was to kidneys. Based on the extrapolated values obtained in OLINDA, the effective dose from ^{177}Lu-**2** to the kidneys would be

1.31 mSv/MBq and 1.14 mSv/MBq for a female and male, respectively (Supplemental Table 4 and 5).

DISCUSSION

There has been an increasingly rapid growth in the field of radiotheranostics, fueled in part by the many successful clinical outcomes, significant investments by the pharmaceutical industry, and also recent regulatory approvals (*27*). Numerous novel radiotheranostics for a wide range of clinically relevant targets are now under investigation (*28*). Here we describe the development of peptide-based radiotheranostics to target the integrin $\alpha_v\beta_6$, an epithelial-specific receptor that been identified as a relevant molecular target for both the detection and treatment of cancer (*29*). Several $\alpha_v\beta_6$-targeting imaging agents have demonstrated utility in the clinic for a range of carcinomas including, breast, colon, head and neck, lung, and pancreas (*16-19*). Based on the functional relevance of this integrin $\alpha_v\beta_6$ it is anticipated that it will become an important target for future radiotheranostics (*30*).

Building on over a decade of research and development of $\alpha_v\beta_6$-targeted peptides for imaging by our group we designed and report herein a radiotheranostic strategy using gallium-68 for PET imaging and lutetium-177 for both treatment and imaging with SPECT. We developed DOTA-5G (**1**), a peptide with high affinity and selectivity for the integrin $\alpha_v\beta_6$, and, with the goal to increase tumor uptake and reduce renal retention, further incorporated a 4-(*p*-iodophenyl)butyryl-containing ABM - based on prior literature showing favorable pharmacokinetics for targeting ligands such as folates, octreotides and PSMA agent phosphoramidates (*31-33*) - to yield DOTA-ABM-5G (**2**). Given the notable presence of the integrin $\alpha_v\beta_6$ in PDAC we evaluated **1** and **2** in a pancreatic mouse model (*11,34,35*).

^{nat}Ga-**1**, ^{nat}Ga-**2**, ^{nat}Lu-**1** and ^{nat}Lu-**2** demonstrated high affinity and selectivity for the integrin $\alpha_v\beta_6$, similar to our previously published $\alpha_v\beta_6$-targeting peptides (*23,26*). Tumors were clearly detectable with ^{68}Ga-**1** and ^{68}Ga-**2** by PET (Figure 3A) and showed uptake similar to other ^{68}Ga-peptides reported in the literature (*19,36*). Both ^{68}Ga-**1** and ^{68}Ga-**2** show predominantly renal excretion, as commonly reported for radiolabeled peptides (*37,38*). Compared to ^{68}Ga-**2**, ^{68}Ga-**1** was cleared quickly from the blood and other non-target tissues,

including healthy pancreas (Figure 3D), resulting in improved contrast. These data reaffirmed our previous reports that although the inclusion of an ABM into targeting ligands increases circulation and tumor uptake, this might not be desirable for short-lived (diagnostic) radioisotopes such as gallium-68 (*39*) or fluorine-18 (*23*). Overall, ^{68}Ga-**1** compare favorably to other noteworthy examples including, ^{68}Ga-cycratide (*36*), ^{68}Ga-DOTA-SFITGv6 (*16*), and ^{68}Ga-Trivehexin (*19*) and was therefore chosen as the clinical candidate for PET imaging.

In vitro studies showed $\alpha_v\beta_6$-targeted cell binding and internalization with minimal efflux of the ^{177}Lu-**2** from cells. ^{177}Lu-**2** also demonstrated good stability (>97% at 24 h) in human serum. Compared to ^{177}Lu-**1**, the addition of the ABM expectedly resulted in longer circulation of ^{177}Lu-**2**, which, in combination with the long half-life of 6.7 days for lutetium-177, was highly beneficial as demonstrated by the biodistribution studies (Figure 5). Lu-**2** was rapidly taken up by and retained in the tumor over the 72 h window, along with significant wash out from all key organs over this time-frame. By the 72 h-time point, only the kidneys showed higher uptake of ^{177}Lu-**2** than the tumor; notably, no renal clearing agents were used in this preclinical study. To further mitigate the high kidney activity, other complementary approaches such as co-injection of positively charged amino acids such as lysine and arginine and pre-targeting will be explored. Biodistribution data were extrapolated to obtain estimated human dosimetry using OLINDA/EXM1.1, showing the highest dose to kidney - as expected from the imaging and biodistribution data - at 1.31 mSv/MBq (female) and 1.14 mSv/MBq (male). These values are considerably lower than those reported for other ^{177}Lu-compounds currently under investigation in the clinic (e.g.: CTT1403, an agent for the treatment of prostate cancer was reported as 5.18 mSv/MBq (*40*)). For ^{177}Lu-**2** the estimated dose would equate to approximately a 1.21 Gy (female) and a 1.05 Gy (male) dose to the kidneys based on a 925 MBq (25 mCi) starting injected dose for our proposed clinical trial, and is significantly lower than the current 23 Gy threshold.

Based on the *in vitro* and *in vivo* data, it was hypothesized that significant tumor killing could be achieved due to selective uptake and trapping of ^{177}Lu-**2** in $\alpha_v\beta_6$ (+) cells; therefore the therapeutic efficacy of ^{177}Lu-**2** was evaluated in the BxPC-3 tumor xenograft model. Two treatment doses were tested, a high single dose of 74 MBq, and a fractioned dose of 2 times 37 MBq, 7 days apart. Both cohorts showed significantly

increased survival above the control groups. While all mice in the control groups had reached end point criteria by day 68, the mice in the treatment groups had 80-86% survival rates at that time point, and showed 1.5-2.0 fold increased median survival times compared to the controls. Importantly, mice in both treatment groups maintained healthy weight during the course of the study, confirming no adverse effects due to either the single (74 MBq) or fractionated double dose (2 × 37 MBq) of ^{177}Lu-**2** (Supplemental Figure 4). These results were highly encouraging, and also contrary to the recently published data by Huynh et al. that reported severe weight loss and death due to kidney toxicity within the first 14 days in mouse cohorts receiving 37 MBq dose of [^{177}Lu]Lu-IBA-DOTA-(PEG28)$_2$-A20FMDV2 (*35*).

Overall, the relevance of integrin $\alpha_v\beta_6$ in cancer, the high binding of ^{177}Lu-**2** to the integrin $\alpha_v\beta_6$, its excellent stability in human serum, along with the therapeutic efficacy and favorable estimated dosimetry collectively suggest the utility of ^{177}Lu-**2** as a therapeutic. ^{177}Lu-**2** was therefore selected as the treatment candidate for our first-in-human radiotheranostics study alongside ^{68}Ga-**1** as imaging agent (NCT04665947).

CONCLUSION

^{68}Ga-**1** and ^{177}Lu-**2** demonstrated high affinity (low nM) and selectivity for the integrin $\alpha_v\beta_6$ both in *in vitro* assays and *in vivo* mouse models, are rapidly internalized, and are stable in human serum. Both radiotracers showed favorable pharmacokinetics in preclinical studies, with predominantly renal excretion and good tumor-to-organ ratios. Favorable human dosimetry data calculated based on the murine biodistribution data for ^{177}Lu-**2** suggest the potential for this treatment. Based on these data, a first-in-human study in patients with locally advanced or metastatic pancreas cancer is underway.

DISCLOSURE

The authors declare the following competing financial interest(s): S. H. Hausner is a co-inventor of intellectual property related to **1** and **2**. J. L. Sutcliffe is founder and CEO of and holds owner-ship interest (including patents) in Luminance Biosciences, Inc., and is a co-inventor of intellectual property related to **1** and **2**. The funding agencies had no role in the design of the study, in the collection, analyses, or interpretation of data, in the writing of the manuscript, or in the decision to publish the results.

ACKNOWLEDGEMENT

This work was supported by Stand Up To Cancer and Lustgarten Foundation Pancreatic Cancer Collective (PCC) New Therapies Challenges (SU2C-AACR-PCC-06-18). We thank the Center for Molecular and Genomic Imaging at UC Davis staff (Charles Smith and Sarah Tam) for their technical support.

KEY POINTS

QUESTION: Can ^{68}Ga- and ^{177}Lu-radiolabeled integrin $\alpha_v\beta_6$-targeting peptides detect and treat $\alpha_v\beta_6$ cancers?

PERTINENT FINDINGS: ^{68}Ga-radiolabeled integrin $\alpha_v\beta_6$-targeting peptides could detect $\alpha_v\beta_6$ positive tumors and the ^{177}Lu-radiolabeled $\alpha_v\beta_6$-targeting peptide ^{177}Lu-**2** demonstrated therapeutic efficacy in a pancreas cancer mouse model.

IMPLICATIONS FOR PATIENT CARE; This ^{68}Ga-/^{177}Lu-radiolabeled $\alpha_v\beta_6$-targeting theranostic pair holds significant promise for patients with locally advanced or metastatic pancreas cancer as well as other $\alpha_v\beta_6$ positive solid tumors.

REFERENCES

1. Siegel RL, Miller KD, Jemal A. Cancer statistics, 2018. 2018;68:7-30.

2. Thomas JK, Kim MS, Balakrishnan L, et al. Pancreatic cancer database: an integrative resource for pancreatic cancer. *Cancer Biol Ther.* 2014;15:963-967.

3. Berghoff AS, Kovanda AK, Melchardt T, et al. alphavbeta3, alphavbeta5 and alphavbeta6 integrins in brain metastases of lung cancer. *Clin Exp Metastasis.* 2014;31:841-851.

4. Allen MD, Marshall JF, Jones JL. alphavbeta6 Expression in myoepithelial cells: a novel marker for predicting DCIS progression with therapeutic potential. *Cancer Res.* 2014;74:5942-5947.

5. Yang GY, Guo S, Dong CY, et al. Integrin alphavbeta6 sustains and promotes tumor invasive growth in colon cancer progression. *World J Gastroenterol.* 2015;21:7457-7467.

6. Niu J, Li Z. The roles of integrin alphavbeta6 in cancer. *Cancer Lett.* 2017;403:128-137.

7. Peng C, Zou X, Xia W, et al. Integrin alphavbeta6 plays a bi-directional regulation role between colon cancer cells and cancer-associated fibroblasts. *Biosci Rep.* 2018;38:1.

8. Cantor DI, Cheruku HR, Nice EC, Baker MS. Integrin alphavbeta6 sets the stage for colorectal cancer metastasis. *Cancer Metastasis Rev.* 2015;34:715-734.

9. Ahmed N, Pansino F, Clyde R, et al. Overexpression of alpha(v)beta6 integrin in serous epithelial ovarian cancer regulates extracellular matrix degradation via the plasminogen activation cascade. *Carcinogenesis.* 2002;23:237-244.

10. Kawashima A, Tsugawa S, Boku A, et al. Expression of alphav integrin family in gastric carcinomas: increased alphavbeta6 is associated with lymph node metastasis. *Pathol Res Pract.* 2003;199:57-64.

11. Reader CS, Vallath S, Steele CW, et al. The integrin alphavbeta6 drives pancreatic cancer through diverse mechanisms and represents an effective target for therapy. *Nat Commun.* 2019;249:332-342.

12. Herrmann K, Schwaiger M, Lewis JS, et al. Radiotheranostics: a roadmap for future development. *Lancet Oncol.* 2020;21:e146-e156.

13. Jadvar H, Chen X, Cai W, Mahmood U. Radiotheranostics in Cancer Diagnosis and Management. *Radiology.* 2018;286:388-400.

14. Maqsood MH, Tameez Ud Din A, Khan AH. Neuroendocrine Tumor Therapy with Lutetium-177: A Literature Review. *Cureus.* 2019;11:e3986.

15. Sun M, Niaz MO, Nelson A, Skafida M, Niaz MJ. Review of 177Lu-PSMA-617 in Patients With Metastatic Castration-Resistant Prostate Cancer. *Cureus.* 2020;12:e8921.

16. Flechsig P, Lindner T, Loktev A, et al. PET/CT Imaging of NSCLC with a α(v)β(6) Integrin-Targeting Peptide. *Mol Imaging Biol.* 2019;21:973-983.

17. Hausner SH, Bold RJ, Cheuy LY, Chew HK, Daly ME, Davis RA. Preclinical Development and First-in-Human Imaging of the Integrin α(v)β(6) with [(18)F]α(v)β(6)-Binding Peptide in Metastatic Carcinoma. *Clin Can Res.* 2019;25:1206-1215.

18. Nakamoto R, Ferri V, Duan H, et al. Pilot-phase PET/CT study targeting integrin α(v)β(6) in pancreatic cancer patients using the cystine-knot peptide-based (18)F-FP-R(0)1-MG-F2. *Eur J Nucl Med Mol Imaging.* 2021; doi: 10.1007/s00259-021-05595-7

19. Quigley NG, Steiger K, Hoberück S, et al. PET/CT imaging of head-and-neck and pancreatic cancer in humans by targeting the "Cancer Integrin" αvβ6 with Ga-68-Trivehexin. *Eur J Nucl Med Mol Imaging.* 2022;49:1136-1147.

20. Lukey PT, Coello C, Gunn R, et al. Clinical quantification of the integrin αvβ6 by [(18)F]FB-A20FMDV2 positron emission tomography in healthy and fibrotic human lung (PETAL Study). *Eur J Nucl Med Mol Imaging.* 2020;47:967-979.

21. Hausner SH, Bauer N, Hu LY, Knight LM, Sutcliffe JL. The Effect of Bi-Terminal PEGylation of an Integrin alphavbeta(6)-Targeted (1)(8)F Peptide on Pharmacokinetics and Tumor Uptake. *J Nucl Med.* 2015;56:784-790.

22. Hausner SH, Abbey CK, Bold RJ, et al. Targeted in vivo imaging of integrin alphavbeta6 with an improved radiotracer and its relevance in a pancreatic tumor model. *Cancer Res.* 2009;69:5843-5850.

23. Hausner SH, Bauer N, Davis RA, Ganguly T, Tang SYC, Sutcliffe JL. The Effects of an Albumin Binding Moiety on the Targeting and Pharmacokinetics of an Integrin alphavbeta6-Selective Peptide Labeled with Aluminum [(18)F]Fluoride. *Mol Imaging Biol.* 2020;22:1543-1552.

24. Hausner SH, DiCara D, Marik J, Marshall JF, Sutcliffe JL. Use of a peptide derived from foot-and-mouth disease virus for the noninvasive imaging of human cancer: generation and evaluation of 4-[18F]fluorobenzoyl A20FMDV2 for in vivo imaging of integrin alphavbeta6 expression with positron emission tomography. *Cancer Res.* 2007;67:7833-7840.

25. Hausner SH, Bauer N, Sutcliffe JL. In vitro and in vivo evaluation of the effects of aluminum [^{18}F]fluoride radiolabeling on an integrin αvβ$_6$-specific peptide. *Nucl Med Biol.* 2014;41:43-50.

26. Ganguly T, Bauer N, Davis RA. Evaluation of Copper-64-Labeled α(v)β(6)-Targeting Peptides: Addition of an Albumin Binding Moiety to Improve Pharmacokinetics. 2021;18:4437-4447.

27. Bodei L, Herrmann K, Schöder H, Scott AM, Lewis JS. Radiotheranostics in oncology: current challenges and emerging opportunities. *Nature Rev Clin Onc.* 2022;19:534-550.

28. Rangger C, Haubner R. Radiolabelled Peptides for Positron Emission Tomography and Endoradiotherapy in Oncology. *Pharmaceuticals (Basel).* 2020;13:22.

29. Bandyopadhyay A, Raghavan S. Defining the role of integrin alphavbeta6 in cancer. *Curr Drug Targets.* 2009;10:645-652.

30. Steiger K, Quigley NG, Groll T, et al. There is a world beyond αvβ3-integrin: Multimeric ligands for imaging of the integrin subtypes αvβ6, αvβ8, αvβ3, and α5β1 by positron emission tomography. *EJNMMI Res.*2021;11:106.

31. Rousseau E, Lau J, Zhang Z, et al. Effects of adding an albumin binder chain on [(177)Lu]Lu-DOTATATE. *Nucl Med Biol.* 2018;66:10-17.

32. Lau J, Jacobson O, Niu G, Lin KS. Bench to Bedside: Albumin Binders for Improved Cancer Radioligand Therapies. *Bioconj Chem.* 2019;30:487-502.

33. Brandt M, Cardinale J, Giammei C, et al. Mini-review: Targeted radiopharmaceuticals incorporating reversible, low molecular weight albumin binders. *Nucl Med Biol.* 2019;70:46-52.

34. Tummers WS, Farina-Sarasqueta A, Boonstra MC, et al. Selection of optimal molecular targets for tumor-specific imaging in pancreatic ductal adenocarcinoma. *Oncotarget.* 2017;8:56816-56828.

35. Huynh TT, Sreekumar S, Mpoy C, Rogers BE. Therapeutic Efficacy of 177Lu-Labeled A20FMDV2 Peptides
Targeting αvβ6. *Pharmaceuticals.* 2022;15:229.

36. Feng X, Wang Y, Lu D, et al. Clinical Translation of a (68)Ga-labeled Integrin αvβ6-targeting Cyclic Radiotracer for PET Imaging of Pancreatic Cancer. *J Nucl Med.*2020;61:1461-1467.

37. de Jong M, Breeman WA, Bernard BF, et al. [177Lu-DOTA(0),Tyr3] octreotate for somatostatin receptor-targeted radionuclide therapy. *Int J Cancer.* 2001;92:628-633.

38. Notni J, Reich D, Maltsev OV, et al. In Vivo PET Imaging of the Cancer Integrin alphavbeta6 Using (68)Ga-Labeled Cyclic RGD Nonapeptides. *J Nucl Med.* 2017;58:671-677.

39. Farkas R, Siwowska K, Ametamey SM, Schibli R, van der Meulen NP, Muller C. (64)Cu- and (68)Ga-Based PET Imaging of Folate Receptor-Positive Tumors: Development and Evaluation of an Albumin-Binding NODAGA-Folate. *Mol Pharm.* 2016;13:1979-1987.

40. Ling X, Latoche JD, Choy CJ, et al. Preclinical Dosimetry, Imaging, and Targeted Radionuclide Therapy Studies of Lu-177-Labeled Albumin-Binding, PSMA-Targeted CTT1403. 2020;22:274-284.

Graphical Abstract

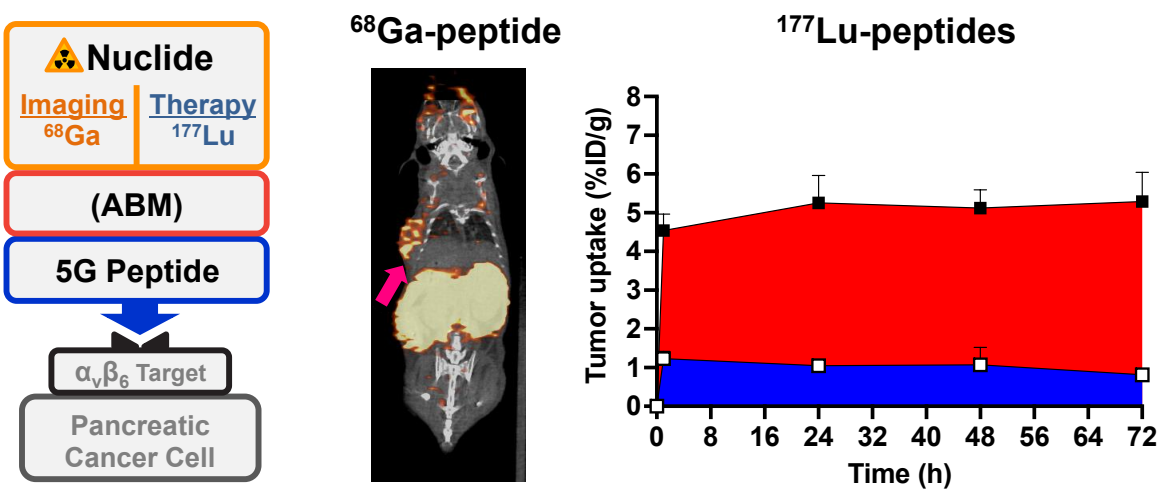

Supplemental Information

Preclinical evaluation of ^{68}Ga- and ^{177}Lu-labeled integrin $\alpha_v\beta_6$-targeting theranostic peptides

Tanushree Ganguly[1], Nadine Bauer[2], Ryan A. Davis[1], Cameron C. Foster[3], Rebecca E. Harris[2], Sven H. Hausner[2], Emilie Roncali[1,3], Sarah Y. Tang[2], Julie L. Sutcliffe[1, 2, 4]

1. *Department of Biomedical Engineering; University of California Davis, Davis, CA, USA*
2. *Department of Internal Medicine, Division of Hematology/Oncology; University of California Davis, Sacramento, CA, USA*
3. *Department of Radiology, Division of Nuclear Medicine; University of California Davis, Sacramento, CA, USA*
4. *Center for Molecular and Genomic Imaging; University of California Davis, Davis, CA, USA*

Table of contents:

Section 1: General information:

Materials and methods

Solvents and chemicals were purchased from Aldrich (Milwaukee, WI, USA) unless stated otherwise and used without further purification. 9-Fluorenylmethoxycarbonyl (Fmoc)-protected amino acids, Novasyn TGR R resin and coupling reagents were purchased from NovaBiochem (San Diego, CA, USA) or GL Biochem (Shanghai, China). Monodisperse Fmoc-amino-PEG-propionic acid (Fmoc-PEG-carboxylic acid; FW= 1544.8 g/mol) was purchased from Polypure (Oslo, Norway). The chelator DOTA tris(*tert*-butyl ester) was purchased from CheMatech (Dijon, France). A reversed-phase (RP) high-performance liquid chromatography (HPLC; Beckman Coulter Gold HPLC) system with an ultraviolet (UV) absorbance detector (220 nm) was used to analyze and purify the peptides. The radiolabeled peptides were analyzed using an analytical radio-HPLC (Beckman Coulter Gold HPLC), serially equipped with a UV absorbance detector (UV, 220 nm) and a radioactivity detector (photomultiplier tube, PMT). The mobile phase was trifluoroacetic acid in water (0.05% v/v; solvent A) and 100% acetonitrile (solvent B). For the analytical HPLC a Phenomenex (Torrence, CA, USA) Jupiter 4 μm Proteo 90 Å column (250 × 4.6 mm, 4 μm) was used with solvent B isocratic 9% for 2 min, then a linear gradient to 81% over 30 min with a flow rate of 1.5 mL/min. For the semi-preparative purification of ^{68}Ga-**1** and ^{68}Ga-**2**, reverse phase HPLC with a Phenomenex Jupiter C18 column (250 x 10 mm, 10 μm) on a Shimadzu system equipped with a 5 mL loop at 1.5 mL/min flow rate was used with a gradient solvent system that started at 35% absolute ethanol in acidified water containing 0.05% hydrochloric acid (HCl), that was held for 1 minute before ramping to 60% absolute

ethanol over 10 minutes and holding it for 5 minutes before ramping back to 35% absolute ethanol. Mass spectrometry was performed at the UC Davis Mass Spectrometry Facility using an UltraFlextreme matrix-assisted laser desorption-ionization time of flight/time of flight (MALDI TOF/TOF) spectrometer (Bruker, Billerica, MA, USA). Centrifree Ultrafiltration devices were purchased from Millipore Sigma (St. Louis, MO, USA). Roswell Park Memorial Institute (RPMI) 1640 medium, fetal bovine serum (FBS), Penicillin-Streptomycin-Glutamine (PSG), and phosphate buffered saline (PBS) were purchased from Gibco/Thermo Fisher (Waltham, MA, USA). Growth factor reduced (GFR) Matrigel was purchased from Corning (Corning, NY, USA).

Cell labeling and biodistribution samples were analyzed with a Wizard 2470 or Wizard 1470 gamma counter (Perkin-Elmer, Waltham, MA, USA). Small-animal PET scans were acquired on an Inveon DPET scanner and computed tomography (CT) scans on a combined high-resolution Inveon SPECT/CT system (Siemens Medical Solutions USA, Knoxville, TN, USA). The data were processed using Siemens Inveon Research Workplace software.

Section 2: Chemistry and radiochemistry

Synthesis and characterization of 1 and 2 and their respective ^{nat}Ga and ^{nat}Lu analogs

Synthesis of DOTA-5G **(DOTA-PEG$_{28}$-GNGVPNLRGDLQVLGQRVGRT-PEG$_{28}$-NH$_2$)** (**1**) - The synthesis of DOTA-5G was performed on solid phase as previously described for NOTA- $\alpha_v\beta_6$-BP using DOTA-tris(*tert*-butyl ester) as the chelator. Following removal of the *N*-terminal Fmoc protecting group from the fully protected 5G peptide (1 equiv) using 20% piperidine (v/v in DMF), the DOTA-tris(*tert*-butyl ester) (3 equiv) was coupled using 1-[bis(dimethylamino)methylene]-1H-1,2,3-triazolo[4,5-b]pyridinium 3-oxide hexafluorophosphate (HATU) (2.8 equiv) and diisopropylethylamine (DIPEA) base (6 equiv) in dimethlyformamide (DMF). The protecting groups were removed and DOTA-5G was cleaved from the resin using trifluoroacetic acid (TFA)/ethanedithiol/water/triisopropylsilane (94:2.5:2.5:1 v/v/v/v) at ambient temperature for 3 h. Pure product was isolated using analytical RP-HPLC and characterized by MALDI mass spectrometry. The analytical data are: HPLC retention time (R_t) = 14.45 min; MALDI m/z = 5199.9468 [M+H$^+$], calculated M+H ($C_{226}H_{422}N_{41}O_{93}$) = 5198.9553.

Synthesis of DOTA-ABM-5G (**2**) - The synthesis of DOTA-ABM-5G was performed on solid phase as previously described for NOTA-K(ABM)-$\alpha_v\beta_6$-BP, using the DOTA-tris(*tert*-butyl ester) chelator as described in the synthesis of **1**. The product was characterized by MALDI mass spectrometry. The analytical data are: HPLC R_t = 17.07

min; MALDI m/z = 5801.0646 [M+H$^+$], calculated M+H ($C_{250}H_{455}IN_{45}O_{98}$) = 5799.0997.

Synthesis of ^{nat}Ga-**1**, ^{nat}Ga-**2**, ^{nat}Lu-**1** and ^{nat}Lu-**2** – For ^{nat}Ga-**1** and ^{nat}Ga-**2**, peptides **1** and **2** (0.4 mg and 0.6 mg, respectively, 1 mM solution in de-ionized water) were mixed with 0.1 mL or 0.055 mL $^{nat}Ga(NO_3)_3$ (2 mM), respectively, stirred at 50°C for 30 min, and purified by analytical RP-HPLC to yield ^{nat}Ga-**1** and ^{nat}Ga-**2**.

For ^{nat}Lu-**1** and ^{nat}Lu-**2**, peptides **1** and **2** (0.8 mg and 0.88 mg respectively, 2 mM solution in de-ionized water) were mixed with 0.15 mL or 0.1 mL $^{nat}LuCl_3$ (4 mM) respectively, stirred at 90°C for 30 min, and purified by analytical RP-HPLC to yield ^{nat}Lu-**1** and ^{nat}Lu-**2**.

The analytical data are: ^{nat}Ga-**1**, HPLC R_t = 14.49 min; MALDI m/z = 5265.1677 [M+H$^+$], calculated M+H$^+$ ($C_{226}H_{419}GaN_{41}O_{93}$) = 5264.8677. ^{nat}Ga-**2**, HPLC R_t = 15.65 min; MALDI m/z = 5866.0694 [M+H$^+$], calculated M+H$^+$ ($C_{250}H_{452}GaIN_{45}O_{99}$) = 5865.0013. ^{nat}Lu-**1**, HPLC R_t = 14.58 min; MALDI m/z = 5371.1171 [M+H$^+$], calculated M+H$^+$ ($C_{226}H_{419}LuN_{41}O_{93}$) = 5370.8721. ^{nat}Lu-**2**, HPLC R_t = 16.63 min; MALDI m/z analysis = 5972.5701 [M+H$^+$], calculated M+H$^+$ ($C_{250}H_{452}ILuN_{45}O_{99}$) = 5971.0165.

Radiolabeling of 1 and 2 with gallium-68 (^{68}Ga-1, ^{68}Ga-2) and lutetium-177 (^{177}Lu-1, ^{177}Lu-2)

Gallium-68 was eluted from a ^{68}Ge/^{68}Ga generator ((Eckert and Ziegler, Berlin, Germany) using 5 mL of 0.1 N HCl, and 1.5 mL fraction containing the bulk radioactivity was used. Radiolabeling was conducted at pH 4.0 in 1M HEPES buffer. Peptide **1** (78 μg) or **2** (80 μg) was mixed with the [^{68}Ga]$GaCl_3$ (333 MBq) eluate in the

reaction vessel. The mixture was heated in the sealed vessel at 90°C for 15 min and purified by semi-preparative HPLC; the product peak was collected, diluted in 15 mL water and loaded on to a C-18 SepPak light cartridge (Waters, Milford, MA, USA). The cartridge was washed with water, dried with air, and the product eluted with 1.5 mL EtOH. The product was dried under a stream of nitrogen gas at 50°C, and formulated in PBS for use. The average decay corrected radiochemical yields for ^{68}Ga-**1** and ^{68}Ga-**2** were 45 % (98% RCP) and 53 % (99% RCP), respectively. The products were characterized by radio-HPLC: ^{68}Ga-**1** co-eluted with the cold standard at 9.09 min and ^{68}Ga-**2** at 9.59 min.

Radiolabeling of peptides **1** and **2** with lutetium-177 (ITM (Garching, Germany) was conducted at pH 5.0 in 0.1 M sodium acetate buffer by adding **1** (44 μg) or **2** (46 μg) to [^{177}Lu]$LuCl_3$ (a 148 MBq aliquot of the commercial [^{177}Lu]$LuCl_3$ in 0.04 N HCl in 100-150 μL buffer) and ascorbic acid (25 μL of a 5 mg/mL aq. solution). The mixture was heated in the sealed vessel at 95°C for 15 min. The radiochemical purity was monitored by i-TLC (TEC-control/BIODEX, solvent phase: 0.1M trisodium citrate) as well as the radio-HPLC method described above. The average decay corrected radiochemical yields for ^{177}Lu-**1** and ^{77}Lu -**2** were 99 % (98% RCP) and 99 % (97% RCP), respectively. The final product was formulated without further purification in PBS for use. The products were characterized by radio-HPLC: ^{177}Lu -**1** co-eluted with the cold standard at 16.39 min and ^{177}Lu -**2** at 17.82 min.

Section 3: *In vitro* experimental details.

The BxPC-3 cells were purchased from American Type Culture Collection (ATCC, Manassas, VA, USA) and cultured at 37°C and 5% CO_2 in RPMI media containing 10% FBS and 1% PSG. All immunohistochemistry supplies were purchased from Vector Labs (Burlingame, CA, USA) unless otherwise stated.

ELISA (IC_{50} determinations).

Competitive binding ELISAs were performed to evaluate the half-maximum inhibitory concentration (IC_{50}) of each peptide relative to each integrin's biotinylated natural ligand (transforming growth factor beta 1 latency-associated peptide, TGFβ1-LAP, G&P Biosciences, Santa Clara, CA, USA) for integrin $\alpha_v\beta_6$ and vitronectin (Thermo Fisher) for integrin $\alpha_v\beta_3$ as previously described. In brief, anti-α_v antibody (P2W7, 5 μg/mL, Abcam, MA, USA) was plated in a 96 well Nunc immune Maxisorp plate (50 μL/well) at 37°C for 1 h, washed with PBS (3x), and blocked overnight with blocking buffer (300 μL/well, 0.5% w/v non-fat dry milk powder (Raley's, West Sacramento, CA, USA), 1% v/v Tween 20, in PBS), followed by washing with PBS (3x). Purified integrin (R&D Systems, MN, USA) in conjugate buffer (50 μL/well, 20 mM Tris, 1 mM $MnCl_2$, 150 mM NaCl, 0.1% v/v Tween 20, 0.1% w/v milk powder in water) was then added to each well, incubated at 37°C for 1 h, followed by washing using wash buffer (20 mM Tris, 1 mM $MnCl_2$, 150 mM NaCl, 0.1% v/v Tween 20 in water, 3x). Serial dilutions of each peptide (10 μM – 10 pM or 100 μM – 100 pM in conjugate buffer) and biotinylated natural ligand were premixed in equal volumes (99 μL each), and added to each well (a total volume of 50 μL/well; n = 3 wells/peptide concentration/biotinylated natural

ligand). Triplicate wells containing no peptide, no peptide and no antibody, or no peptide and no ligand served as controls. The plate was incubated at 37°C for 1 h, then washed with wash buffer (3x). A 1:1000 dilution of ExtrAvidin Horseradish Peroxidase (HRP, Thermo Fisher) was added to each well (50 µL/well), incubated at 37°C for 1 h, and then washed with wash buffer (3x). The ExtrAvidin HRP was detected with TMB One solution (50 µL/well) (Promega Corporation, Madison, WI, USA) for 10 – 15 min at room temperature. The reaction was stopped by adding 1N H_2SO_4 (50 µL/well) and the absorbance was measured in a Multiscan Ascent plate reader (Thermo Fisher) at 450 nm. The IC_{50} of the peptides was determined by fitting to a sigmoidal dose-response model in GraphPad Prism 8.0 (GraphPad, CA, USA).

Cell Binding and Internalization.

Prior to the experiment, the cell lines were analyzed by flow cytometry to confirm levels of integrin expression. For cell binding experiments 7.4 kBq aliquots of ^{68}Ga-**1** and ^{177}Lu -**2** in 50 µL serum free medium (pH 7.2) were added to a cell suspension (3.75×10^6 cells in 50 µL serum free media) and incubated for 1 h at room temperature in closed microfuge tubes (n = 3/cell line/compound). The tubes, pretreated with non-fat dry milk powder (0.5% w/v in PBS) to block nonspecific binding, were regularly agitated to prevent settling of the cells. Following centrifugation at 130 × g for 3 min, the supernatant was removed and the cell pellet was washed with 0.5 mL serum free RPMI. The corresponding supernatants were combined, and the cells re-suspended in 0.6 mL serum free medium. The fraction of bound radioactivity was determined with a γ-counter (cell pellet vs. combined supernatants). To determine the fraction of internalized

radioactivity at the 60 min time point, the cells were subsequently treated with acidic wash buffer (0.2 M sodium acetate, 0.5 M sodium chloride, pH 2.5, 300 µL, 4°C, 5 min) to release surface-bound activity, followed by a wash with PBS (300 µL). The internalized fraction was determined with a γ-counter (cell pellet vs. radioactivity released into supernatant). Samples from the ^{177}Lu-**2** experiment were further analyzed to determine the efflux of internalized ^{177}Lu-**2**. The pellet was suspended in 0.3 mL of serum-free RPMI, incubated at 37°C, and the supernatant collected at 0.25 h and 1 h, respectively, and the pellet washed with another 0.3 mL of PBS. At each time point, the respective supernatant and wash were combined, and the pellet was suspended in 0.6 mL PBS. The fraction of retained activity in the pellet was determined with a γ-counter (cell pellet vs. combined supernatants).

Albumin Binding.

Binding of the radiotracers ^{177}Lu-**1** and ^{177}Lu-**2** to serum proteins was evaluated by ultrafiltration using Centrifree Ultrafiltration devices according to the manufacturer's recommendations. Experiments were carried out in quadruplicate. The devices were pre-treated with PBS containing Tween 20 (5% v/v), followed by triplicate rinses with PBS. An aliquot of each formulated radiotracer in PBS (≤25 µL, 20-60 KBq) was thoroughly mixed with 0.5 mL serum at 37°C in a microfuge tube. The mixture was incubated at 37°C for 5 min and an aliquot (50 µL) of was transferred to a tube for γ-counting. The remaining sample was transferred to a Centrifree Ultrafiltration device and centrifuged for 40 min at 1500 × g at ambient temperature (20-24°C). An aliquot (50 µL) of the filtrate was transferred to a tube for γ-counting. For each radiotracer, a blank was run

using 0.5 mL PBS / Tween 20 (5% v/v) instead of serum (n = 4) to determine non-specific binding. Following γ-counting, the protein-bound radioactivity was calculated by subtracting the counts measured in the filtrate aliquot (i.e.: not protein bound) from the counts in the corresponding serum aliquot. The data are expressed as mean ± standard deviation of fraction of radioactivity bound to protein after subtraction of non-specific binding determined in the blank.

Serum Stability

Mouse or human serum (500 µL, both Millipore Sigma) was combined with an aliquot of the formulated radiotracer (3.7 - 7.4 MBq) and incubated at 37°C. Aliquots (100–200 µL) were drawn for analysis at 1 and 2 h for the gallium-68 radiotracers and 1 and 24 h for lutetium-177 radiotracers, mixed with absolute ethanol (500 µL, 4°C), and centrifuged (2300 × g, 3 min) to precipitate out serum proteins. The supernatant was diluted with HPLC solvent A, and analyzed by radio-HPLC to determine the fraction of intact radiotracer as previously described in Section 2.

Section 4: Biodistribution

Gallium-68 was eluted from a 1850 MBq ^{68}Ge/^{68}Ga generator (Eckert and Ziegler, Berlin, Germany) and non-carrier added (n.c.a.) lutetium-177 was obtained from ITM (Garching, Germany).

For small animal imaging, aliquots of the formulated radiotracers (^{68}Ga-**1** or ^{68}Ga-**2**, 7.4–9.25 MBq in 150 µL PBS; pH 7.2; molar activity at injection = 7.4-7.8 GBq/µmol)

were injected intravenously (i.v.) via a catheter into the tail vein of mice (n = 3/time point/radiotracer) anesthetized with 2–3% isoflurane in medical grade oxygen. Animals were imaged in a prone position on the scanner bed. Anesthesia was maintained during the scan at 1.5–2.5% isoflurane. Static, single-frame 15-min emission scans at 1 and 2 h post injection (p.i.) was acquired for both radiotracers. CT scans for anatomical reference was acquired post the PET scans at each time point.

For biodistribution, the radiotracers (3.0-3.7 MBq in 100 µL PBS; pH 7.2; molar activity at injection = 6.6-11.1 GBq/µmol (^{68}Ga-**1** or ^{68}Ga-**2**); molar activity at injection = 18.5 GBq/µmol (^{177}Lu-**1** and ^{177}Lu -**2**)) were injected into the tail vein of mice (n = 3/time point/radiotracer) anesthetized with 2–3% isoflurane, followed by conscious uptake periods of 1 and 2 h (^{68}Ga-**1**), 2 and 4 h (^{68}Ga-**2**), or 1, 24, 48, and 72 h (^{177}Lu-**1** and ^{177}Lu -**2**). At each time point, the mice were anesthetized and sacrificed, the tissues collected, rinsed with PBS, and the radioactivity of each measured with a gamma counter. Calibrated, decay-corrected radioactivity concentrations are expressed as percent of injected dose per gram of tissue (% ID/g).

	^{68}Ga-**1** (%ID/g)		^{68}Ga-**2** (%ID/g)	
Tissue	**1 h**	**2 h**	**2 h**	**4 h**
Blood	0.34 ± 0.27	0.09 ± 0.01	8.89 ± 0.89	5.72 ± 0.78
Gall Bladder	4.58 ± 7.02	0.49 ± 0.12	1.91 ± 1.10	2.70 ± 2.64
Liver	0.14 ± 0.09	0.11 ± 0.02	1.46 ± 0.16	1.36 ± 0.02
Heart	0.46 ± 0.12	0.27 ± 0.02	3.24 ± 0.35	2.28 ± 0.35
Lung	2.68 ± 0.91	1.87 ± 0.12	6.08 ± 0.11	6.41 ± 1.03
Spleen	0.09 ± 0.04	0.03 ± 0.00	1.55 ± 0.18	1.02 ± 0.11
Kidneys	23.34 ± 3.31	13.83 ± 3.91	19.62 ± 2.83	25.92 ± 2.24
Pancreas	0.17 ± 0.05	0.10 ± 0.02	1.37 ± 0.36	1.08 ± 0.12
Stomach	3.61 ± 0.55	2.75 ± 0.63	9.72 ± 1.29	11.80 ± 0.65
Sm Intestines	2.12 ± 0.42	1.27 ± 0.16	6.38 ± 0.43	7.70 ± 0.45
Bladder	36.23 ± 52.45	0.98 ± 0.4	7.81 ± 3.46	11.05 ± 11.19
Skin	0.93 ± 0.29	0.74 ± 0.25	4.10 ± 0.60	3.94 ± 0.78
Muscle	0.47 ± 0.14	0.34 ± 0.08	1.66 ± 0.44	1.15 ± 0.10
Bone	0.27 ± 0.04	0.45 ± 0.35	1.55 ± 0.33	0.93 ± 0.36
Lg Intestines	2.75 ± 1.04	2.08 ± 0.21	7.42 ± 0.83	8.73 ± 0.11
Brain	0.03 ± 0.01	0.02 ± 0.00	0.31 ± 0.02	0.18 ± 0.04
BxPC-3	2.60 ± 0.80	2.03 ± 0.57	9.39 ± 1.89	10.35 ± 2.58

Supplemental Table 1. Biodistribution of ^{68}Ga-**1** and ^{68}Ga-**2** in mice bearing $\alpha_v\beta_6$ (+) BxPC-3 tumors (n = 3/group/time point). Uptake data are expressed as decay-corrected percentage of injected dose per gram of tissue [%ID/g].

	^{177}Lu-**1** (%ID/g)			
	1 h	**24 h**	**48 h**	**72 h**
Blood	0.10 ± 0.03	0.00 ± 0.00	0.00 ± 0.00	0.00 ± 0.00
Gall Bladder	0.71 ± 0.40	0.61 ± 0.59	0.88 ± 0.83	0.42 ± 0.43
Liver	0.10 ± 0.03	0.06 ± 0.01	0.0 5± 0.00	0.04 ± 0.00
Heart	0.35 ± 0.04	0.14 ± 0.01	0.13 ± 0.03	0.10 ± 0.03
Lung	1.19 ± 0.18	0.53 ± 0.06	0.36 ± 0.09	0.27 ± 0.05
Spleen	0.05 ± 0.02	0.02 ± 0.00	0.02± 0.00	0.02 ± 0.00
Kidneys	12.23 ± 3.91	9.54 ± 2.33	7.52 ± 2.65	6.16 ± 1.45
Pancreas	0.41 ± 0.38	0.16 ± 0.03	0.13 ± 0.04	0.09 ± 0.00
Stomach	4.10 ± 0.98	2.55 ± 0.52	1.84 ± 0.08	0.95 ± 0.13
Sm Intestines	2.18 ± 0.33	0.82 ± 0.05	0.40 ± 0.06	0.13 ± 0.02
Bladder	3.83 ± 2.75	0.93 ± 0.29	0.89 ± 0.17	0.71 ± 0.24
Skin	0.75 ± 0.08	0.58 ± 0.09	0.41 ± 0.11	0.23 ± 0.06
Muscle	0.43 ± 0.05	0.18 ± 0.05	0.13 ± 0.01	0.11 ± 0.07
Bone	0.17 ± 0.13	0.11 ± 0.02	0.09 ± 0.02	0.06 ± 0.01
Lg Intestines	3.98 ± 0.62	1.95 ± 0.22	1.31 ±0.40	0.46 ± 0.03
Brain	0.01 ± 0.00	0.01 ± 0.00	0.01 ± 0.00	0.01 ± 0.00
BxPC-3	1.23 ± 0.19	1.05 ± 0.11	1.07 ± 0.45	0.81 ± 0.16

Supplemental Table 2. Biodistribution of ^{177}Lu-**1** in mice bearing $\alpha_v\beta_6$ (+) BxPC-3 tumors (n = 3/time point). Uptake data are expressed as decay-corrected percentage of injected dose per gram of tissue [%ID/g].

	^{177}Lu-2 (%ID/g)			
	1 h	**24 h**	**48 h**	**72 h**
Blood	5.36 ± 0.71	0.08 ± 0.01	0.02 ± 0.00	0.01 ± 0.00
Gall Bladder	1.72 ± 0.46	1.11 ± 0.71	0.71 ± 0.13	1.09 ± 0.61
Liver	1.05 ± 0.05	0.22 ± 0.01	0.16 ± 0.02	0.12 ± 0.01
Heart	2.05 ± 0.37	0.71 ± 0.05	0.64 ± 0.06	0.46 ± 0.11
Lung	2.68 ± 0.21	1.10 ± 0.15	0.68 ± 0.08	0.53 ± 0.10
Spleen	0.75 ± 0.03	0.12 ± 0.01	0.10 ± 0.02	0.10 ± 0.01
Kidneys	20.89 ± 3.10	12.34 ± 1.24	10.14 ± 1.04	8.84 ± 1.15
Pancreas	0.92 ± 0.07	0.60 ± 0.11	0.50 ± 0.09	0.36 ± 0.12
Stomach	9.16 ± 0.58	7.55 ± 1.45	5.49 ± 0.27	4.76 ± 1.22
Sm Intestines	5.46 ± 0.54	3.02 ± 0.32	1.74 ± 0.22	0.71 ± 0.16
Bladder	6.75 ± 2.39	2.91 ± 0.16	2.69 ± 0.33	3.29 ± 0.63
Skin	2.16 ± 0.35	1.49 ± 0.57	0.95 ± 0.05	1.08 ± 0.16
Muscle	0.96 ± 0.24	0.52 ± 0.08	0.52 ± 0.03	0.42 ± 0.02
Bone	0.66 ± 0.15	0.27 ± 0.08	0.16 ± 0.19	0.19 ± 0.13
Lg Intestines	6.31 ± 1.86	3.63 ± 0.09	3.13 ± 0.53	3.01 ± 0.44
Brain	0.14 ± 0.01	0.04 ± 0.01	0.02 ± 0.00	0.03 ± 0.00
BxPC-3	4.54 ± 0.42	5.25 ± 0.71	5.12 ± 0.47	5.29 ± 0.75

Supplemental Table 3. Biodistribution of ^{177}Lu-**2** in mice bearing $\alpha_v\beta_6$ (+) BxPC-3 tumors (n = 3/time point). Uptake data are expressed as decay-corrected percentage of injected dose per gram of tissue [%ID/g].

Section 5: Blocking

For blocking studies, 8.3 μmol/kg of peptide **1** (30 mg/kg) (before ^{68}Ga-**1** or ^{177}Lu-**1**) or **2** (48 mg/kg) (before ^{77}Lu-**2**) was injected 10 min before the respective formulated radiotracer, for the mice bearing BxPC-3 tumors. The tissues were collected 1 h (^{68}Ga-**1** and ^{177}Lu-**1**) or 4 h (^{77}Lu-**2**) p.i., rinsed with PBS, and the radioactivity of each measured with a gamma counter. Calibrated, decay-corrected radioactivity concentrations are expressed as percent of injected dose per gram of tissue (% ID/g).

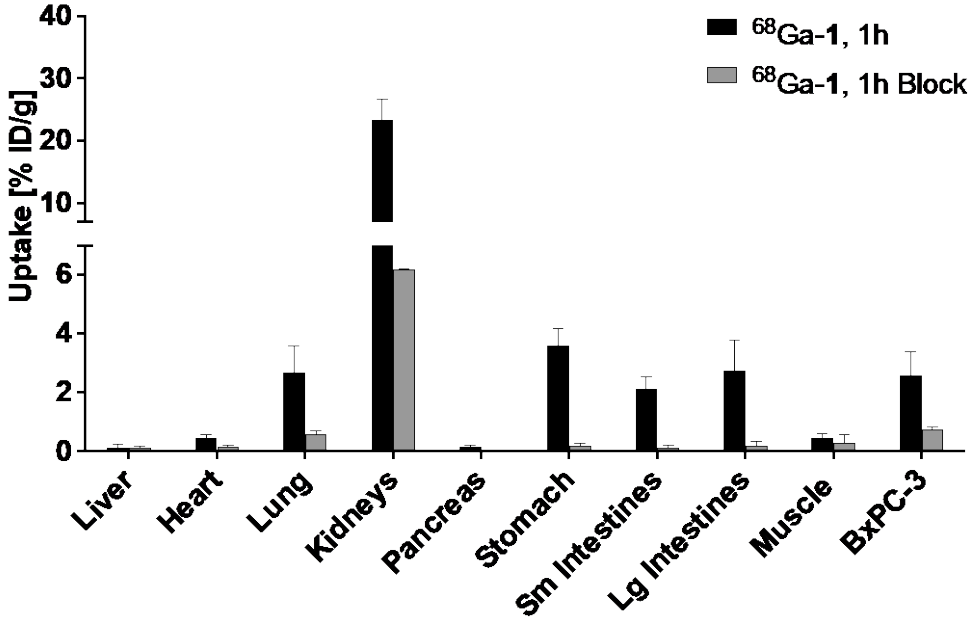

Supplemental Figure 1. Biodistribution of ^{68}Ga-**1** in mice bearing $\alpha_v\beta_6$ (+) BxPC-3 tumors at 1 h p.i. (unblocked: n = 3, blocked: n = 2). Uptake data are expressed as decay-corrected percentage of injected dose per gram of tissue (Columns: uptake [% ID/g]; bars: SD)

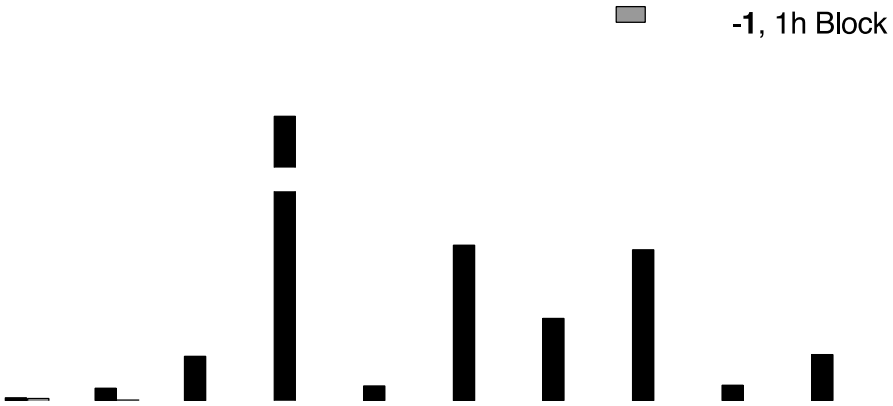

Supplemental Figure 2. Biodistribution of ^{177}Lu-**1** in mice bearing $\alpha_v\beta_6$ (+) BxPC-3 tumors at 1 h p.i. (unblocked: n = 3, blocked: n = 2). Uptake data are expressed as decay-corrected percent of injected dose per gram of tissue (Columns: uptake [% ID/g]; bars: SD)

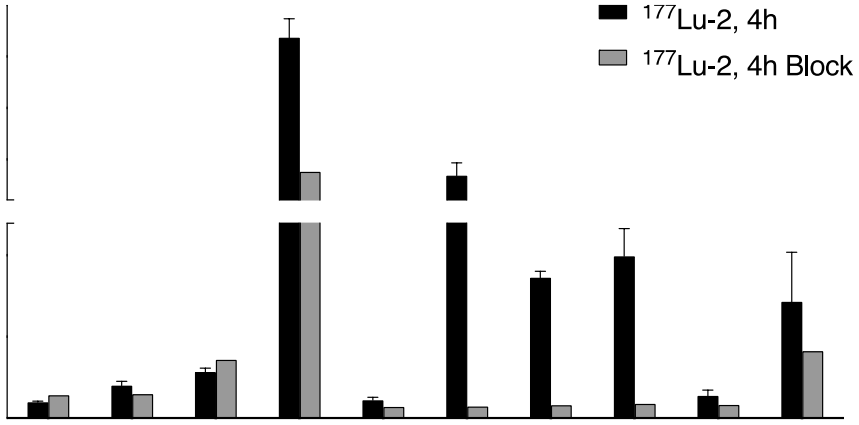

Supplemental Figure 3. Biodistribution of ^{177}Lu-**2** in mice bearing $\alpha_v\beta_6$ (+) BxPC-3 tumors at 4 h p.i. (unblocked: n = 3, blocked: n = 1). Uptake data are expressed as decay-corrected percentage of injected dose per gram of tissue (Columns: uptake [% ID/g]; bars: SD)

Section 6: Dosimetry

The human dosimetry estimates for ^{177}Lu-**2** were computed using OLINDA/EXM1.1 based on the activity concentration (% ID) obtained for various organs in the extended mouse biodistribution study (n=4/sex/time point; 24 h, 48 h, 72 h, 1 week, and 2 weeks). A bi-exponential fit was used for all organs and the time activity curves were generated using OLINDA/EXM 1.1 using a female or male model with organ mass scaling . Effective doses are reported in mSv/MBq.

Target Organ	Alpha	Beta	Photon	Total	EDE Cont.	ED Cont.
Adrenals	0.00E+00	0.00E+00	4.79E-03	4.79E-03	0.00E+00	1.20E-05
Brain	0.00E+00	1.22E-03	5.38E-05	1.28E-03	0.00E+00	3.19E-06
Breasts	0.00E+00	0.00E+00	2.87E-04	2.87E-04	4.31E-05	1.44E-05
Gallbladder Wall	0.00E+00	8.06E-03	3.02E-03	1.11E-02	0.00E+00	0.00E+00
LLI Wall	0.00E+00	3.43E-02	1.14E-03	3.54E-02	2.12E-03	4.25E-03
Small Intestine	0.00E+00	1.81E-02	2.09E-03	2.02E-02	0.00E+00	5.05E-05
Stomach Wall	0.00E+00	1.97E-01	6.74E-03	2.04E-01	1.23E-02	2.45E-02
ULI Wall	0.00E+00	2.20E-02	2.27E-03	2.43E-02	0.00E+00	6.08E-05
Heart Wall	0.00E+00	2.94E-02	1.41E-03	3.08E-02	1.85E-03	0.00E+00
Kidneys	0.00E+00	1.28E+00	2.32E-02	1.31E+00	7.84E-02	3.27E-02
Liver	0.00E+00	1.34E-02	2.38E-03	1.58E-02	0.00E+00	7.89E-04
Lungs	0.00E+00	1.43E-02	9.32E-04	1.53E-02	1.83E-03	1.83E-03
Muscle	0.00E+00	2.84E-04	7.91E-04	1.07E-03	0.00E+00	2.69E-06
Ovaries	0.00E+00	0.00E+00	1.04E-03	1.04E-03	2.59E-04	2.08E-04
Pancreas	0.00E+00	1.54E-01	6.27E-03	1.60E-01	9.60E-03	4.00E-04
Red Marrow	0.00E+00	0.00E+00	1.09E-03	1.09E-03	1.31E-04	1.31E-04
Osteogenic Cells	0.00E+00	4.27E-04	1.12E-03	1.54E-03	4.63E-05	1.54E-05
Skin	0.00E+00	0.00E+00	3.01E-04	3.01E-04	0.00E+00	3.01E-06
Spleen	0.00E+00	1.13E-02	4.93E-03	1.63E-02	0.00E+00	4.06E-05
Thymus	0.00E+00	0.00E+00	3.10E-04	3.10E-04	0.00E+00	7.74E-07
Thyroid	0.00E+00	0.00E+00	6.19E-05	6.19E-05	1.86E-06	3.09E-06
Urinary Bladder Wall	0.00E+00	2.22E-02	1.04E-03	2.32E-02	0.00E+00	1.16E-03
Uterus	0.00E+00	0.00E+00	8.54E-04	8.54E-04	0.00E+00	2.13E-06
Total Body	0.00E+00	8.11E-03	9.65E-04	9.07E-03	0.00E+00	0.00E+00
Effective Dose Equivalent (mSv/MBq)					1.07E-01	
Effective Dose (mSv/MBq)						6.62E-02

Supplemental Table 4. Human dosimetry female estimates for ^{177}Lu-**2**. Effective dose values are expressed in mSv/MBq.

Target Organ	Alpha	Beta	Photon	Total	EDE Cont.	ED Cont.
Adrenals	0.00E+00	0.00E+00	3.62E-03	3.62E-03	0.00E+00	9.04E-06
Brain	0.00E+00	8.13E-04	4.03E-05	8.53E-04	0.00E+00	2.13E-06
Breasts	0.00E+00	0.00E+00	2.61E-04	2.61E-04	3.92E-05	1.31E-05
Gallbladder Wall	0.00E+00	4.81E-03	2.76E-03	7.57E-03	0.00E+00	0.00E+00
LLI Wall	0.00E+00	2.35E-02	7.81E-04	2.43E-02	0.00E+00	2.91E-03
Small Intestine	0.00E+00	1.36E-02	1.47E-03	1.51E-02	0.00E+00	3.78E-05
Stomach Wall	0.00E+00	1.43E-01	4.72E-03	1.48E-01	8.86E-03	1.77E-02
ULI Wall	0.00E+00	1.45E-02	1.70E-03	1.62E-02	0.00E+00	4.05E-05
Heart Wall	0.00E+00	2.99E-02	1.28E-03	3.12E-02	1.87E-03	0.00E+00
Kidneys	0.00E+00	1.12E+00	2.05E-02	1.14E+00	6.83E-02	2.85E-02
Liver	0.00E+00	3.48E-02	2.88E-03	3.77E-02	2.26E-03	1.89E-03
Lungs	0.00E+00	1.21E-02	7.47E-04	1.29E-02	1.55E-03	1.55E-03
Muscle	0.00E+00	1.58E-04	6.24E-04	7.83E-04	0.00E+00	1.96E-06
Ovaries	0.00E+00	0.00E+00	7.06E-04	7.06E-04	1.77E-04	1.41E-04
Pancreas	0.00E+00	6.83E-02	4.32E-03	7.26E-02	4.36E-03	1.82E-04
Red Marrow	0.00E+00	0.00E+00	9.14E-04	9.14E-04	1.10E-04	1.10E-04
Osteogenic Cells	0.00E+00	4.18E-04	8.63E-04	1.28E-03	3.84E-05	1.28E-05
Skin	0.00E+00	0.00E+00	2.48E-04	2.48E-04	0.00E+00	2.48E-06
Spleen	0.00E+00	6.59E-03	3.67E-03	1.03E-02	0.00E+00	2.56E-05
Testes	0.00E+00	0.00E+00	8.72E-05	8.72E-05	0.00E+00	0.00E+00
Thymus	0.00E+00	0.00E+00	3.01E-04	3.01E-04	0.00E+00	7.54E-07
Thyroid	0.00E+00	0.00E+00	5.22E-05	5.22E-05	1.56E-06	2.61E-06
Urinary Bladder Wall	0.00E+00	2.41E-02	8.35E-04	2.50E-02	0.00E+00	1.25E-03
Uterus	0.00E+00	0.00E+00	6.55E-04	6.55E-04	0.00E+00	1.64E-06
Total Body	0.00E+00	6.47E-03	7.80E-04	7.25E-03	0.00E+00	0.00E+00
Effective Dose Equivalent (mSv/MBq)					8.76E-02	
Effective Dose (mSv/MBq)						5.44E-02

Supplemental Table 5. Human dosimetry male estimates for ^{177}Lu-**2**. Effective dose values are expressed in mSv/MBq.

Section 7: Therapy

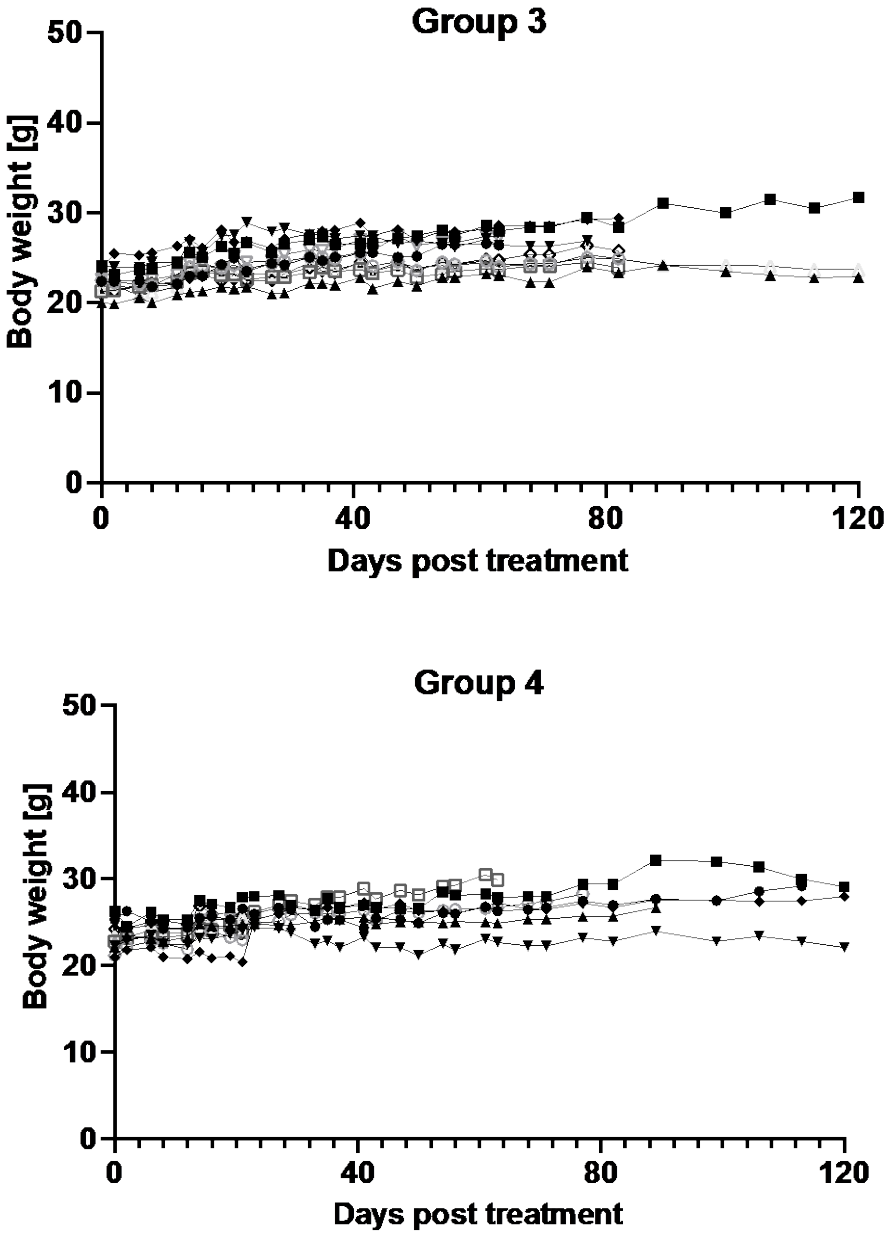

Supplemental Figure 4. Body weight measurements throughout the duration of the therapy study (1-2 times per week for up to 120 days) for treatment Group 3 (74 MBq ^{177}Lu-**2**) and Group 4 (2 × 37 MBq ^{177}Lu-**2**).